Investigating the Feasibility of Utilizing Electrical Arc Furnace Slag and Circulating Dry Scrubber Dust as Binder for Cemented Paste Backfill

Noureddine Ouffa[1], Tikou Belem[1], Romain Trauchessec[2], André Lecomte[2], and Mostafa Benzaazoua[3]

[1]Research Institute of Mines and Environment, Université du Québec en Abitibi-Témiscamingue, Rouyn-Noranda, PQ, Canada, noureddine.ouffa@uqat.ca; tikou.belem@uqat.ca
[2]Université de Lorraine, CNRS, Institut Jean Lamour, Nancy, France, romain.trauchessec@univ-lorraine.fr
[3]Geology and Sustainable Mining Department, Mohammed VI Polytechnic University, Ben Guerir, Morocco, Mostafa.BENZAAZOUA@um6p.ma

Abstract

In the Abitibi-Témiscamingue mining region in Canada, underground mines utilize cemented paste backfill (CPB) for secondary ground support. The conventional CPB formulation employs a binder known as the reference binder (RB), consisting of 20% general use Portland cement (GU) and 80% ground granulated blast furnace slag (GGBFS). This reference binder (RB = 20 GU/80 GGBFS) demonstrates excellent mechanical and hydro-geotechnical properties for CPB. However, its high cost, limited availability of GGBFS, and the environmental impact associated with GU production highlight the critical need for research into alternative, cost-effective, and environmentally friendly binders.This study explores the use of electrical arc furnace slag (EAFS) and circulating dry scrubber dust (CDSD) from the steelmaking industry to partially replace GGBFS and act as a substitute for GU cement. The EAFS undergoes a processing stage involving screening and grinding, resulting in a product termed ground EAFS (GEAFS). Various formulations of the ternary blended binder (GGBFS/GEAFS/CDSD) are evaluated for their unconfined compressive strength (UCS) at 7 and 28 days to assess their suitability as binders for CPB. Our results demonstrate the feasibility of completely replacing type GU cement and substituting up to 30% of GGBFS in the RB without compromising the UCS at 28 days (UCS_{28d}). These highly promising findings suggest the potential to lower the cost and carbon footprint of CPB while promoting the recycling of metallurgical waste within the mining industry, aligning with a circular economy approach.

Key words: cemented paste backfills, eco-friendly binders, ground granulated blast furnace slag, electric arc furnace slag, circulating dry scrubber dusts, binder cost, carbon footprint reduction

Introduction

In the Quebec economy, the mining sector plays a crucial role by supplying essential metals, valuable minerals, creating employment opportunities, and contributing important government revenue. In 2020, the mining activities in Quebec made a noteworthy impact on the Gross Domestic Product (GDP), amounting to approximately 12.9 billion C$, with 10.5 billion C$ specifically attributed to Quebec. In the Abitibi-Témiscamingue region, these mining activities contributed about 22.8% of total employment and approximately 35.8% of the regional GDP in the same year, as reported by Ecotec Consultants (2022). However, a notable challenge arises from the substantial volume of mine tailings generated by the mining industry. Traditionally, these tailings are managed in storage facilities, incurring economic drawbacks. The associated costs include those related to development, construction, maintenance, monitoring, and rehabilitation of these facilities (Bussière and Guittonny, 2020; Carneiro and Fourie, 2019). Furthermore, this practice raises environmental concerns, encompassing issues related to land usage and water pollution

(Elghali et al., 2023). Additionally, there are geotechnical risks associated with the potential failure of these tailings' storage facilities (Bowker and Chambers, 2015).

The introduction of CPB technology represents an innovative alternative for handling mine tailings in the mining sector. CPB is composed of filtered mine tailings, constituting 70–85% of the total CPB by weight, plus hydraulic binders (2–10% dry tailings weight), and mixing water from sources such as lakes, tap or processed water. This technology provides a comprehensive, secure, and sustainable approach to mine tailings management (Belem and Benzaazoua, 2003; Benzaazoua et al., 2003). In certain instances, additional components like crushed waste rocks (Hane et al., 2017) and additives (Ouattara et al., 2018) are integrated to enhance particle size distribution, consistency, and setting time. These additives may include superplasticizers and set-controlling admixtures, such as accelerators or retarders. The incorporation of such elements contributes to optimizing the overall performance of the CPB technology in tailings management. Commonly employed binders in mine tailings management include GU, either alone or blended with supplementary cementitious materials (SCMs). These SCMs often consist of GGBFS, a byproduct of cast iron, or various types of fly ashes (FA-F, FA-C) derived from thermal power processes (Tariq and Yanful, 2013).

On average, the expenses related to binders constitute approximately 75% of the costs in backfilling operations, where backfill costs in turn make up 10–20% of the total expenses in mining operations (Gauthier, 2004; Grice, 1998). In the Abitibi-Témiscamingue region of Québec, Canada, RB is a prevalent binder (Belem et al., 2010). While the RB consistently meets the mechanical strength and hydro-geotechnical requirements for ground control (Benzaazoua et al., 2002; Godbout et al., 2007; Sahi, 2016; Yilmaz et al., 2010; Yilmaz et al., 2011), challenges arise due to its high cost (Curry, 2020a; Curry, 2020b), limited availability of GGBFS (Scrivener et al., 2018), and environmental impacts associated with GU production (Chen et al., 2010). Consequently, there is a compelling need for research aimed at identifying alternative, cost-effective, and environmentally friendly binders in the field of mine tailings management.

Ouffa et al. (2023) have showcased the effectiveness of utilizing circulating dry scrubber dust (CDSD) as an activator for GGBFS. CDSD, an alkaline waste with a pH > 12, is a finely textured by-product consisting of calcium sulfites ($CaSO_3.x(H_2O)$), calcium hydroxide or portlandite ($Ca(OH)_2$), and gypsum ($CaSO_4.2H_2O$). This by-product originates from the steel production processes employed at the RioTinto iron and titanium (RTIT) steel works in Sorel-Tracy city, Québec, Canada. CDSD has demonstrated its viability as a substitute for sodium hydroxide (NaOH) and GU in activating GGBFS. Notably, CDSD can function as a complete replacement for GU in the reference binder while still maintaining a relatively comparable unconfined compressive strength at 28 days (UCS_{28d}) when compared to the reference binder. Specifically, the UCS_{28d} for the blended binder with 20% CDSD and 80% GGBFS reaches 2212 ± 134 kPa. In comparison, the UCS_{28d} for the RB stands at 2016 ± 205 kPa. Notably, the unconfined compressive strength at 7 days (UCS_{7d}) for the 20% CDSD/80% GGBFS blend measures at 856 ± 26 kPa, a value considered satisfactory for mining backfill applications, albeit lower than the UCS_{7d} of the reference binder, which achieves 1430 ± 55 kPa. In addressing this, Ouffa et al. (2023) suggest the addition of 5% clinker to the mixture for enhanced UCS_{7d} in mining applications. Moreover, Ouffa et al. (2023) have recommended considering fly ashes type F and fine glass powders as partial substitutes for GGBFS. This study aims to propose another alternative approach by introducing the utilization of EAFS, an industrial

by-product readily available in Quebec pending appropriate treatment. EAFS is produced in Quebec by RioTinto Iron and Titanium in Sorel-Tracy and by ArcelorMittal Long Product Canada in Contrecœur (Quebec, Canada).

EAFS is a byproduct resulting from the steel production process, specifically generated during the refining of steel in an electric arc furnace. This furnace employs high-power electric arcs, facilitated by graphite electrodes, to melt recycled steel scrap and transform it into high-quality steel. Lime is introduced into the scrap materials to facilitate the melting process, and oxygen is injected into the molten metal to oxidize undesirable elements. These oxidized elements then combine with the lime to form slag. As the melting process progresses, liquid steel accumulates at the bottom of the furnace. Once the desired chemical composition of the steel is achieved, the slag and steel are extracted from the furnace. The molten slag is then directed to a specialized slag treatment facility using containers or supports (Shi, 2005; Yildirim and Prezzi, 2011).

The average density of EAFS is 3.35, ranging between 2.8–3.9 (Geiseler, 1996; Teo et al., 2020; Thomas et al., 2019). Its chemical composition can vary, and is primarily composed of oxides such as CaO (2–60%), FeO (2–52%), SiO_2 (6–34%), Al_2O_3 (2–14%), and MgO (3–15%). Additionally, EAFS contains other oxidized impurities like MnO (1–5%), TiO_2 (0–1%), SO_3 (0.1–2%), and P_2O_5 (0.5–2%), along with free lime (f-CaO) and free magnesia (f-MgO) (Thomas et al., 2019; Yildirim and Prezzi, 2011). The primary mineral phases identified in EAFS include belite, larnite or dicalcium silicate (β and γ-Ca_2SiO_4), alite (Ca_3SiO_5), merwinite ($Ca_3Mg(SiO_4)_2$), bredigite ($Ca_7Mg(SiO_4)_4$), gehlenite ($Ca_2Al_2SiO_7$), and wustite (solid solution of FeO) (Brand and Roesler, 2014; Geiseler, 1996; Shi, 2005; Yildirim and Prezzi, 2011).

Since the 1880s, EAFS has been processed and utilized as phosphate fertilizer (Geiseler, 1996), as well as acting as supplementary cementitious materials, aggregates in concrete, contributing to road construction, and participating in cement clinker production (Jiang et al., 2018; Motz and Geiseler, 2001). According to Shi (2005), the cementitious properties of EAFS are associated with the presence of compounds like C_3S ($3CaO.SiO_2$), C_2S ($2CaO.SiO_2$), C_4AF ($4CaO.Al_2O_3.FeO$), and C_2F ($2CaO.FeO$). Additionally, a properly cooled, high-basicity steel slag, as per the same source, can exhibit cementitious properties, albeit generally weaker due to the low C_3S compared to clinker. The limited cementitious properties can be attributed to the high iron oxide content, the highly crystalline nature of EAFS, and the low amounts of SiO_2 and Al_2O (Roslan et al., 2016). As the result, EAFS can only partially substitute Portland cement or blast furnace slag in systems involving GU/GGBFS, GU/FA, or GU/silica fume (SF) (Amin et al., 2015; Cristelo et al., 2023; Shi, 2005). The reported maximum substitution rate stands at 30% (Amin et al., 2015; Muhmood et al., 2009; Ghadimi and Naghipour, 2023; Shi, 2005). Nevertheless, the optimal percentage seems to be 10%, maintaining strengths comparable to those of Portland cement (Amin et al., 2015; Hekal et al., 2013; Roslan et al., 2016; Roslan et al., 2020). Cements containing EAFS demonstrate extended setting times, lower heat release during hydration, enhanced strength development at advanced curing times (> 28 days), and improved sulfate resistance compared to Portland cement (Cristelo et al., 2023; Roslan et al., 2016; Shi, 2005). Their strengths correlate with increased alkalinity (Muhmood et al., 2009; Shi, 2005), prompting the exploration of various treatments to boost the alkalinity of such slag.

Various strategies have been proposed in scientific literature to enhance the reactivity of EAFS, including rapid pressurized water quenching, chemical composition modification, grinding, CO_2 sequestration, and

alkaline activation. Rapid pressurized water quenching has shown potential in improving EAFS reactivity (Muhmood et al., 2009), although it does not significantly alter the mineralogical structure compared to other slag types such as ladle furnace slags (Tossavainen et al., 2007). Kim et al. (2015) suggested a similar approach, involving chemical composition modification to adjust the CaO/Al_2O_3 ratio and reduce the FeO content to 2–5%, thereby enhancing the reactivity of EAFS. Lu et al. (2019) have proposed a method of modifying the chemical composition of EAFS by incorporating various industrial wastes and by-products to increase the CaO/Al_2O_3 basicity index. This modification has been shown to result in the production of modified slag with favorable cementitious properties. In addition, alkaline activation has been identified to enhance EAFS reactivity when combined with other materials like GGBFS or FAF. Other suggested treatments include carbon sequestration (Mahoutian et al., 2015; Mo et al., 2017) and grinding (Sun et al., 2022). According to Roslan et al. (2020), the fine grains of EAFS play a role in bridging the gap between $Ca(OH)_2$, ettringite, and the hard phase.

In the concrete field, EAFS offers interesting characteristics, but these have not been detailed for CPB. Taking into account economic limitations and the diverse treatments outlined in existing literature, this study suggests a partial substitution of GGBFS with sieved and ground EAFS in a CDSD/GGBFS system used as binder for CPB. The proposed ranges drawn from literature review and prior laboratory experiments are: 50% ≤ GGBFS ≤ 70%, 15% ≤ CDSD ≤ 30%, and 5% ≤ sieved and ground EAFS ≤ 20%.

Materials and Methods

The materials employed in this study encompass Sil-Co-Sil 106® procured from US SILICA, GU supplied by McInnis Cement, GGBFS provided by Lafarge Canada Inc., CDSD obtained from Harsco Environmental in Sorel-Tracy (Quebec, Canada) and EAFS supplied by ArcelorMittal Long Product Canada in Contrecœur (Québec, Canada). The EAFS sample under investigation was collected from two furnaces (50% AMOASC + 50% AMEASC). Notably, CDSD is a byproduct resulting from the air desulfurization process at the RioTinto Iron and Titanium metallurgical complex in Sorel-Tracy (Québec, Canada). CDSD and EAFS were acquired through the collaborative effort of the Technology Transfer Center in Industrial Ecology and Université of Québec at Temiscaming.

Sil-Co-Sil 106®, employed as solid skeleton of cemented paste backfill (as a substitute for actual tailings), is a high-purity fine sand consisting of 99.8% silicon oxide (www.ussilica.com). It possesses a relative density (G_s) of 2.65 and a BET specific surface area of 880 m^2/kg. Peyronnard and Benzaazoua (2011) compared the particle size distribution of Sil-Co-Sil 106® with that of a tailings sample from LaRonde (in Abitibi, Quebec, Canada), collected in 2011. This analysis shows that the particle size distribution of Sil-Co-Sil 106® closely mirrors that of tailings from the LaRonde mine

The processing of EAFS involved screening and grinding (Figure 1). Initially, the EAFS underwent primary crushing using a Géliko laboratory jaw crusher in a closed circuit with screening, employing a SWECO vibrating sieve with a diameter $\phi = 2$ mm. A segment of the challenging-to-crush slag ($\phi > 2$ mm) was separated and termed as REAFS. Following the screening, the crushed portion that passed through the sieve underwent a secondary crushing process using a Marcy® Gy-Roll Lab Cone Crusher and a grinding process in a laboratory steel rod mill with a 9 L capacity. The grinding load constituted approximately 25% of grinder volume and consisted of three types of bars: 1/2 in, 3/2 in and 5/2 in.

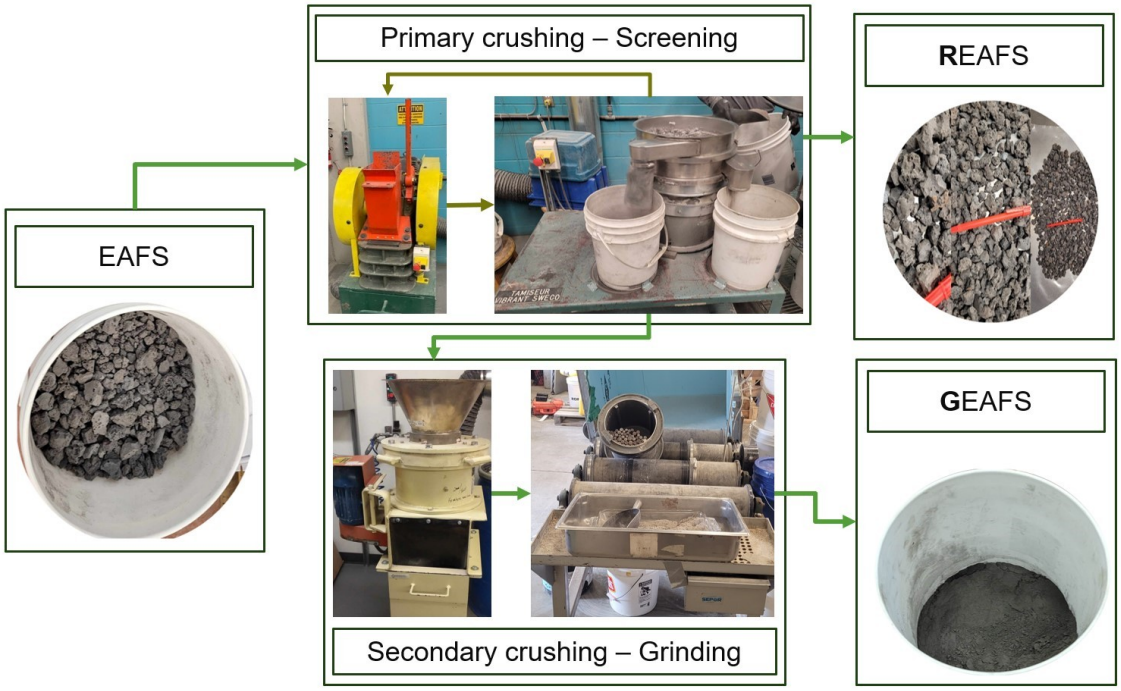

Figure 1. Process of treating and preparing EAFS for utilization as a supplementary cementitious material.

The simulated cemented paste backfill (SCPB) mixture and uniaxial compression tests were conducted on cylindrical specimens with a diameter (d) of 30 mm and a height (h) of 60 mm, resulting in an aspect ratio (h/d) of 2, following the methodology outlined by Ouffa et al. (2023). Notably, the solids mass concentration (C_w) of SCPB was maintained at 75% and the binder ratio (B_w) was set at 7%, equivalent to a binder content (C_c) of 6.54%. The definitions are as follows: $C_w = M_{solid}/M_{SCPB}$, $B_w = M_{binder}/M_{Sil\text{-}Co\text{-}Sil106}$, and $C_c = M_{binder}/(M_{Sil\text{-}Co\text{-}Sil106}+M_{binder}) = B_w/(1+B_w)$. Additionally, statistical analysis of the results using R and Minitab and the calculation of environmental footprints and costs followed the methodology detailed by Ouffa et al. (2023).

We conducted comprehensive characterizations on the investigated cementitious materials encompassing physical, chemical, and mineralogical aspects. Physical characterization involved relative density and specific surface area measurements. Relative density determined using the Micrometrics AccuPyc 1330 helium pycnometer, while specific surface area was assessed via the BET method using the Micrometrics GEMINI surface analyzer, following the approach established by Brunauer, Emmett, and Teller. Chemical characterization comprised sulfur and carbon content measurement using an ELTRA CS-2000 induction furnace with a detection limit of 0.009%, free lime analysis according to the ASTM C 114 standard, and examinations via X-ray fluorescence (XRF) and by inductively coupled plasma mass spectrometry with strong acid digestion. Major elements were determined by XRF using fusion beads method, conducted on a Bruker S8 TIGER spectrometer with fused beads prepared using an automatic fusion machine (Autofluxer®). Minor element analysis was carried out by ICP-MS at SGS Minerals Services Canada in

Lakefield, Ontario. Measurements of sulfur and carbon levels, free lime, and ICP-MS were exclusively performed on the GEAFS sample. The alkalinity of GEAFS and the investigated cementitious materials was calculated using Equation 1:

$$M_{b3} = \frac{\%CaO + \%MgO}{\%SiO_2 + \%Al_2O_3} \quad \text{Equation 1}$$

Table 1 provides the outcomes of both physical and chemical characterization conducted by XRF for the four cementitious materials. In Tables 2 and 3, data elaborates on the ICP-MS analysis and the assessment of sulfur/carbon and free lime content specific to the GEAFS.

Table 1. XRF analysis and physical properties of the cementitious materials.

Oxide	GU	CDSD	GGBFS	GEAFS	REAFS
SiO_2	19.96	2.08	36.84	16.64	18.92
Al_2O_3	4.43	0.64	10.04	6.77	6.24
CaO	64.77	52.60	39.98	29.36	31.25
Fe_2O_3	3.44	0.95	0.69	32.40	27.82
K_2O	0.62	0.05	-	0.10	0.10
MgO	1.78	1.00	11.54	12.01	11.60
MnO	0.06	-	0.22	2.14	3.24
P_2O_5	-	-	0.13	0.86	0.21
Cr_2O_3	-	-	-	0.68	-
SO_3	1.95	32.98	0.56	0.22	0.15
SrO	0.05	0.03	-	-	0.02
TiO_2	0.32	0.45	1.25	1.26	1.42
V_2O_5	-	-	-	0.16	-
ZrO_2	-	-	0.03	-	-
*LOI (950°C)	2.63	9.14	-1.22	-2.69	-3.00
Gs	3.08	2.38	2.88	3.81	-
¶BET SSA (m^2/kg)	1,462.00	13,441.00	2,227.00	1,984.00	-
M_{b3}	-	-	1.10	1.77	1.70

*LOI = loss on ignition; ¶BET SSA = BET method specific surface area

In this investigation, GU and CDSD are classified as activators, while GGBFS and GEAFS fall under the category of activated materials. GU is primarily composed of CaO and SiO_2, making up 85% of its composition, with Al_2O_3 and Fe_2O_3 accounting for 8%. In comparison, CDSD is primarily composed of CaO and SO_3, exhibiting a relative density of 2.38 and significant BET specific surface area. As for GGBFS, it predominantly composed of CaO and SiO_2 in nearly equal proportions ($CaO/SiO_2 \approx 1.1$), making up 77% of its composition. Additionally, GGBFS contains nearly equivalent proportions of Al_2O_3 and MgO ($Al_2O_3/MgO \approx 0.9$), constituting 22%.

Both GEAFS and REAFS showcase nearly identical chemical compositions. GEAFS comprises CaO and Fe_2O_3, with a CaO/Fe_2O_3 ratio of approximately 1 making up 62% of its composition. It also includes SiO_2, MgO, and Al_2O_3, collectively constituting 35%. The primary difference in the XRF chemical compositions of GEAFS and REAFS lies in GEAFS having around -5% Fe_2O_3 relative to REAFS. This indicates a higher iron concentration in the finer fraction, The BET specific surface area of GEAFS exceeds that of GU and closely approaches that of GGBFS. Additionally, GEAFS exhibits an alkalinity index, $M_{b3} > 1$, indicating its potential pozzolanic properties. The free lime (f-CaO) content is 0.12% lower than the specified limit for clinker, which typically ranges from 0.5–1.5% f-CaO (Alemayehu and Sahu, 2013).

Table 2. ICP-MS analysis of GEAFS

Element	**Units**	**Value**	**Element**	**Units**	**Value**
Total Boron	µg/g	66.00	**Manganese**	**%**	**1.40**
Silica	**%**	**7.09**	Molybdenum	µg/g	10.00
Aluminum	**%**	**3.20**	Sodium	µg/g	850.00
Arsenic	µg/g	6.10	Nickel	µg/g	46.00
Barium	µg/g	220.00	Lead	µg/g	14.00
Beryllium	µg/g	1.80	**Sulfur**	**%**	**0.31**
Bismuth	µg/g	0.14	Antimony	µg/g	0.90
Calcium	**%**	**20.00**	Selenium	µg/g	< 0.70
Cadmium	µg/g	0.36	Strontium	µg/g	210.00
Cobalt	µg/g	5.70	Tellurium	µg/g	0.10
Chromium	**%**	**0.20**	Titanium	µg/g	1.00
Copper	µg/g	63.00	Thallium	µg/g	< 0.02
Iron	**%**	**14.00**	Uranium	µg/g	6.10
Potassium	µg/g	280.00	Vanadium	µg/g	360.00
Lithium	µg/g	5.10	Yttrium	µg/g	31.00
Magnesium	**%**	**6.20**	Zinc	µg/g	430.00

Table 3. Sulfur/Carbone and free lime of GEAFS

	C_{total}	S_{total}	f-CaO
	wt.%	wt.%	wt.%
DLM*	0.05	0.009	
GEAFS	0.07	0.044	0.12

*DLM = detection limit of the method

The mineralogical analysis was carried out using XRD with a Bruker A.X.S. Advance D8 apparatus equipped with $Cu_{K\alpha 1}$ radiation (λ = 1.54056 Å). Operational parameters were set at 40 kV and 30 mA, with an increment of 0.54°/min in the 5–70° (2θ) range. Diffractograms were indexed using Diffract Eva 6.0 software along with the PDF 2023 database. Figures 2 and 3 present the indexed diffractograms of the five cementitious materials under investigation.

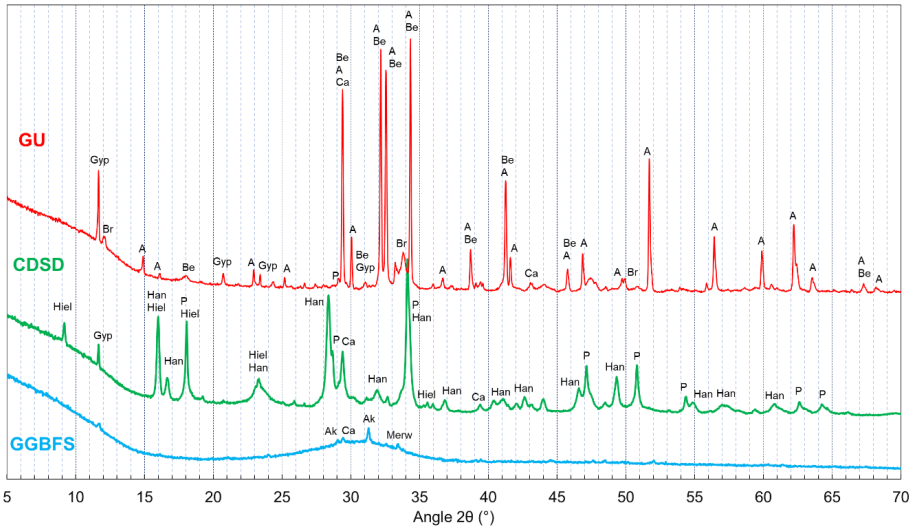

Figure 2. X-ray diffractograms of the GU, CDSD and GGBFS. Abbreviations for minerals are Ak: akermanite; Ca: calcite; Merw: merwinite; Per: periclase; Geh: gehlinite; Wus: wustite; Mag: magnetite; Han: hannebachite; P: portlandite; Hiel: hielscherite; A: alite, Be: belite; Gyp: gypse; Br: brownmerillite.

GGBFS primarily exists in an amorphous state, with minor phases including akermanite ($Ca_2MgSi_2O_7$), calcite, and merwinite $Ca_3Mg(SiO_4)_2$. CDSD is comprised of calcium sulphites (hanebachite $CaSO_3.H_2O$), calcite ($CaCO_3$), calcium hydroxide or portlandite ($Ca(OH)_2$), hielscherite ($Ca_3Si(SO_4)(SO_3)(OH)_6.11H_2O$), and gypsum ($CaSO_4.2H_2O$). GU is composed of alite ($3CaO.SiO_2$), belite ($2CaO.SiO_2$), brownmillerite ($Ca_2(Al,Fe)_2O_5$), and gypsum ($CaSO_4.2H_2O$).

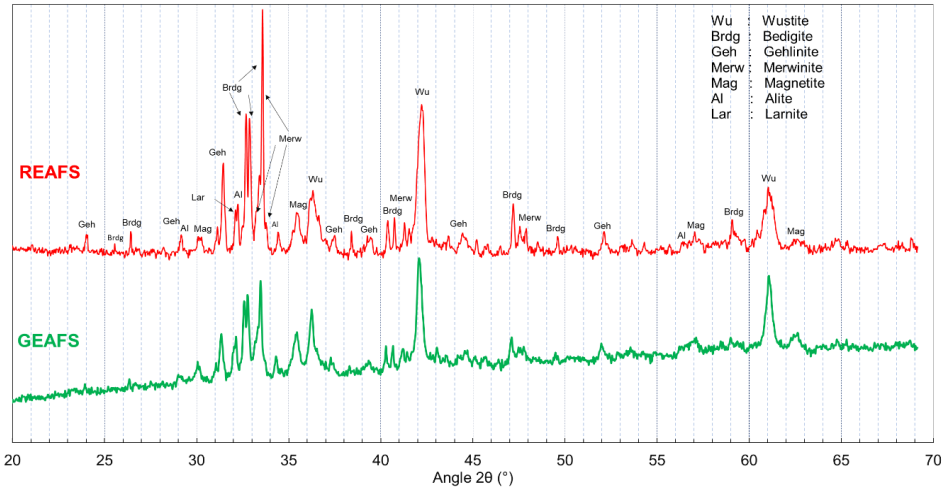

Figure 3. X-ray diffractograms of the GEAFS and REAFS.

In Figure 3, the diffractograms of the two slags (GEAFS and REAFS) exhibit nearly identical peaks, indicating the presence of the same phases. The primary distinction lies in the intensity of these peaks, with GEAFS showing less intense peaks compared to REAFS. This variation could be interpreted as a higher concentration of the amorphous phase in GEAFS. Both GEAFS and REAFS predominantly contain wustite (FeO), magnetite ($Fe^{2+}Fe^{3+}{}_2O_4$), bredegite ($Ca_7Mg(SiO_4)_4$), gehlenite ($Ca_2Al(AlSi)O_7$), merwenite ($Ca_3Mg(SiO_4)_2$), alite (Ca_3SiO_5), and larnite (Ca_2SiO_4). These phases align with those commonly reported in the literature for EAFS (Teo et al., 2020; Yildirim and Prezzi, 2011).

Results and Discussion

Table 4 displays the results of the UCS_{7d} and UCS_{28d} from the SCPB specimens incorporating diverse formulations of ternary binders, consisting of GGBFS, GEAFS, and CDSD.

Table 4. Uniaxial compression test results (UCS) for ternary blends GGBFS-GEAFS-CDSD, with solids mass concentration (C_w) of 75%, binder ratio (B_w) of 7%, binder content (C_c) of 6.54%.

N° Sample	Proportions			UCS_{7d} (kPa)		UCS_{28d} (kPa)	
	GGBFS	GEAFS	CDSD	Mean	Standard deviation	Mean	Standard deviation
RB*	0.80	0.00	**0.2 GU**	1430	55	2016	205
M0S1	0.80	0.00	0.20	856	26	2212	134
M14S1	0.65	0.20	0.15	337	7	2169	81
M14S2	0.65	0.05	0.30	923	23	2295	100
M14S3	0.50	0.20	0.30	736	49	1816	117
M14S4	0.70	0.15	0.15	365	22	2212	83
M14S5	0.70	0.05	0.25	779	17	2316	107
M14S6	0.68	0.05	0.28	786	166	2240	49
M14S7	0.68	0.18	0.15	400	15	2326	37
M14S8	0.70	0.10	0.20	623	26	2493	104
M14S9	0.58	0.20	0.23	621	16	2059	71
M14S10	0.58	0.13	0.30	933	98	2077	67
M14S11	0.64	0.13	0.23	652	4	2153	101
M14S12	0.65	0.17	0.19	487	13	2159	68
M14S13	0.65	0.09	0.27	746	23	2083	72
M14S14	0.57	0.17	0.27	692	25	1947	38
M14S15	0.67	0.14	0.19	492	11	2300	80
M14S16	0.67	0.09	0.24	723	14	2264	76

*RB = reference binder = **0.8GGBFS/0.2GU**

The results reveal UCS_{28d} values that are similar, or even slightly superior, to those of the RB across all formulations. The UCS_{28d} ranges from 1816 ± 117 kPa (for M14S3 mixture: 0.5 GGBFS/0.2 GEAFS/0.3 CDSD) to 2493 ± 104 kPa (for M14S8 mixture: 0.7 GGBFS/0.1 GEAFS/0.2 CDSD). Notably, these two formulations enable the complete substitution of GU and a partial replacement of 30 and 10% in the GGBFS content in the RB, respectively. However, the UCS_{7d} of SCPB specimens based on ternary

mixtures GGBFS/GEAFS/CDSD is lower compared to that of the RB, which exhibits a UCS_{7d} of 1430 ± 30 kPa. The UCS_{7d} of the ternary mixtures ranges from 337 ± 7 kPa (for M14S1 mixture: 0.65 GGBFS/0.2 GEAFS/0.15 CDSD) to 933 ± 98 kPa (for M14S10 mixture: 0.575 GGBFS/0.125 GEAFS/0.3 CDSD). It is noteworthy that most, if not all, of the UCS_{7d} values presented are deemed acceptable in the context of mine backfills.

Within mining sites, the mining operation cycle typically spans approximately one month, representing the duration between the backfilling of primary open stopes and the excavation of secondary stopes. Consequently, UCS_{28d} holds significant importance in this context. In the subsequent part of the study, our aim is to comprehend the impact of each component (ie, GGBSF, GEAFS, and CDSD) on UCS_{28d}.
The analysis of correlations between the various terms of the full cubic model and UCS_{28d} is presented in Table 5. Results indicate a robust positive correlation between GGBFS and UCS_{28d}. Additionally, it is noteworthy that positive correlations exclusively involve GGBFS, while all negative correlations involve GEAFS. Hence, one could infer that the incorporation of GEAFS might have a negative impact on the UCS_{28d} of GGBFS/CDSD binary mixtures (see M0S1 in Table 4).

Table 5. Correlation analysis of UCS_{28d} for ternary mixtures GGBFS/GEAFS/CDSD.

Positive correlations		**Negative correlations**	
Term	R	Term	R
GGBFS	0.90	GEAFS	-0.52
GGBFS×CDSD×(GGBFS–CDSD)	0.78	GEAFS×CDSD	-0.84
		GGBFS× GEAFS×CDSD	-0.78

To validate this hypothesis, UCS_{28d} was underwent modeling using a full cubic model, as detailed in the materials and methods section, and represented by Equation (2) (with a coefficient of determination R^2 = 0.89 and $R^2_{Adjusted}$ = 0.79), where:

$$X_1 = GGBFS;\ X_2 = GEAFS,\ X_3 = CDSD \qquad \text{Equation 2}$$

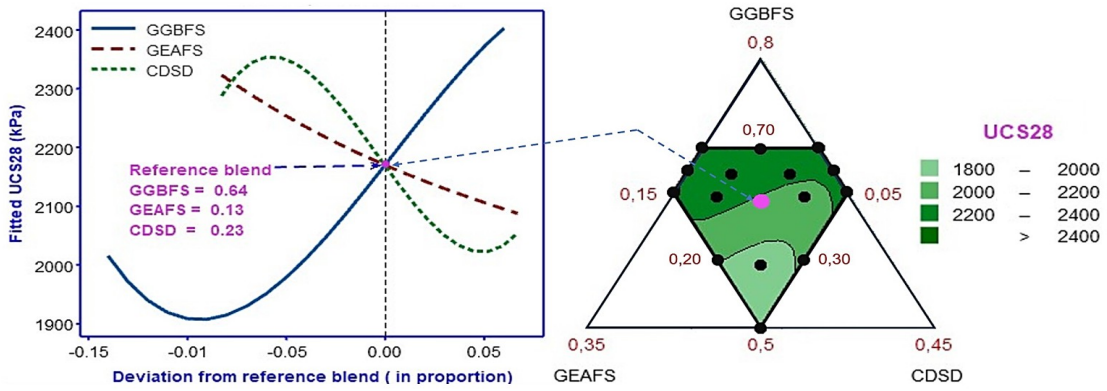

Figure 4. Cox trace plot and ternary diagram illustrating UCS_{28d} (kPa) for the GGBFS/GEAFS/CDSD binder mixtures.

Use of Equation 2 permits the construction of ternary diagram and Cox trace plot (Figure 4). The visual representation clearly illustrates that the incorporation of GEAFS results in a decrease in 28 day strength, following an almost linear trend. However, this reduction is limited to around 200 kPa at most, which is not highly significant when considering the economic advantages of substitution. Additionally, literature sources emphasize that EAFS exhibits reactions over the long term (beyond 28 days and more) as detailed in the literature review (see introduction section). Therefore, it becomes crucial to assess these slags over the long term to ascertain their utility.

Conclusions

The objective of this paper is to showcase the feasibility of utilizing GEAFS as a partial substitute for GGBFS in a CDSD/GGBFS blended binder. CDSD has previously proven successful as an alternative to GU in activating GGBFS, presenting a cost-effective and environmentally friendly option in comparison to the traditional RB. Moreover, both EAFS and CDSD are locally available industrial waste byproducts in Québec, specifically in Sorel-Tracy and Contrecœur. Based on our research, the following conclusions can be drawn:

- achieving UCS_{28d} values comparable to those of the RB without using GU and with reduced costs is a promising outcome from the unconfined compression tests presented in this article
- it is viable to completely substitute GU and decrease the GGBFS content in the RB by up to 30% without significantly impacting UCS_{28d}
- evaluating the long-term reactivity of treated GEAFS in the GGBFS/CDSD system is crucial to determine its suitability as partial replacement for GGBFS on an industrial scale

Finaly, the incorporation of GEAFS as a substitute for GGBFS has the potential to lower the costs and decrease the environmental impact of mining with CPB, especially in Québec where GGBFS is imported while EAFS is locally available.

Acknowledgments

The authors would like to express their gratitude to Mitacs Accelerate (#IT26385) and the Natural Science and Engineering Research Council of Canada (NSERC) for their generous financial support. Special appreciation is extended to Pascal Lemoine and Youssef Benarchid from the Centre de Transfert Technologique en Écologie Industrielle (CTTÉI) for their invaluable assistance in obtaining CDSD and EAFS from RioTinto Iron and Titanium, ArcelorMittal Long Products Canada, and Harsco Environmental. A sincere thanks also go to Lafarge Inc. for providing GGBFS and McInnis Cement for supplying GU Portland cement.

References

Alemayehu, F., & Sahu, O. (2013). Minimization of variation in clinker quality. Advances in Materials, 2(2), 23-28.

Amin, M. S., El-Gamal, S. M. A., Abo-El-Enein, S. A., El-Hosiny, F. I., & Ramadan, M. (2015). Physico-chemical characteristics of blended cement pastes containing electric arc furnace slag with and without silica fume. HBRC Journal, 11(3), 321-327. doi:https://doi.org/10.1016/j.hbrcj.2014.07.002

Belem T., Benzaazoua, M. (2003) Utilisation du remblai en pâte comme support de terrain. Partie I : de sa fabrication à sa mise en place sous terre. Après-mines 2003, "Impacts et gestion des risques: besoins et acquis de la recherché." 5–7 February 2003, Nancy. GISOS, CD-ROM, 12p.

Belem, T., Peyronnard, O., Benzaazoua, M. (2010). A model of formulation of blended binders for use in cemented mine backfills. Proceedings of 1st International Seminar on Reduction of Risk in the Management of Tailings and Mine Waste – Mine Waste'10, Perth, WA, Australia, 29 sept – 1st oct. 2010, pp. 433-448.

Benzaazoua, M., Belem, T., & Bussière, B. (2002). Chemical factors that influence the performance of mine sulphidic paste backfill. Cement and Concrete Research, 32(7), 1133-1144. doi:https://doi.org/10.1016/S0008-8846(02)00752-4

Benzaazoua M., Belem T., Ouellet S., Fall M. (2003) Utilisation du remblai en pâte comme support de terrain. Partie II : comportement à court, à moyen et à long terme. Après-mines 2003, "Impacts et gestion des risques : besoins et acquis de la recherché." 5–7 February 2003, Nancy. GISOS, CD-ROM, 12p.

Bouzoubaâ, N., & Fournier, B. (2005). Current situation with the production and use of supplementary cementitious materials (SCMs) in concrete construction in Canada. Canadian Journal of Civil Engineering, 32(1), 129-143.

Bowker, L. N., & Chambers, D. M. (2015). The risk, public liability, & economics of tailings storage facility failures. Earthwork Act, 24, 1-56.

Brand, A. S., & Roesler, J. R. (2014). Concrete with steel furnace slag and fractionated reclaimed asphalt pavement. Retrieved from: Bussière, B., & Guittonny, M. (2020). Hard rock mine reclamation: from prediction to management of acid mine drainage: CRC press.

Carneiro, A., & Fourie, A. B. (2019). An integrated approach to cost comparisons of different tailings management options. Paper presented at the Paste 2019: Proceedings of the 22nd International Conference on Paste, Thickened and Filtered Tailings, Cape Town. https://papers.acg.uwa.edu.au/p/1910_05_Carneiro/

Chen, C., Habert, G., Bouzidi, Y., & Jullien, A. (2010). Environmental impact of cement production: detail of the different processes and cement plant variability evaluation. Journal of cleaner production, 18(5), 478-485. doi:https://doi.org/10.1016/j.jclepro.2009.12.014

Cristelo, N., Coelho, J., Rivera, J., Garcia-Lodeiro, I., Miranda, T., & Fernández-Jiménez, A. (2023). Application of electric arc furnace slag as an alternative precursor to blast furnace slag in alkaline cements. Journal of Sustainable Cement-Based Materials, 12(9), 1081-1093. doi:10.1080/21650373.2022.2161660

Curry, K. C. (2020a). Cement Statistics and Information. Retrieved from https://www.usgs.gov/centers/nmic/cement-statistics-and-information

Curry, K. C. (2020b). Iron and Steel Slag Statistics and Information. Retrieved from https://www.usgs.gov/centers/nmic/iron-and-steel-slag-statistics-and-information?qt-science_support_page_related_con=0#qt-science_support_page_related_con

EcoTec Consultants. (2022). Retombées économiques de l'industrie minière au Québec en 2020. Retrieved from https://amq-inc.com/contenu/

Elghali, A., Benzaazoua, M., Taha, Y., Amar, H., Ait-khouia, Y., Bouzahzah, H., & Hakkou, R. (2023). Prediction of acid mine drainage: Where we are. Earth-Science Reviews, 241, 104421. doi:https://doi.org/10.1016/j.earscirev.2023.104421

Gauthier, P. (2004). Valorisation des liants et des rejets industriels dans les remblais miniers. Rapport DESS, Université du Québec en Abitbi-Témiscamingue, Rouyn-Noranda, Canada.

Geiseler, J. (1996). Use of steelworks slag in Europe. Waste management, 16(1), 59-63. doi:https://doi.org/10.1016/S0956-053X(96)00070-0

Godbout, J., Bussière, B., Aubertin, M., Belem, T. (2007). Evolution of cemented paste backfill saturated hydraulic conductivity at early curing time. Proceedings of 60th Canadian Geotechnical Conference and the 8th Joint CGS/IAH-CNC Groundwater Conference, Ottawa, 21-24 October 2007, p. 2230-2236.

Grice, T. (1998). Underground mining with backfill. 2nd Annual Summit œ Mine Tailings Disposal Systems, Brisbane, Nov, 24-25.

Hane, I., Belem, T., Benzaazoua, M., & Maqsoud, A. (2017). Laboratory characterization of cemented tailings paste containing crushed waste rocks for improved compressive strength development. Geotechnical and Geological Engineering, 35, 645-662.

Hekal, E. E., Abo-El-Enein, S. A., El-Korashy, S. A., Megahed, G. M., & El-Sayed, T. M. (2013). Hydration characteristics of Portland cement – Electric arc furnace slag blends. HBRC Journal, 9(2), 118-124. doi:10.1016/j.hbrcj.2013.05.006

Jiang, Y., Ling, T.-C., Shi, C., & Pan, S.-Y. (2018). Characteristics of steel slags and their use in cement and concrete—A review. Resources, Conservation and Recycling, 136, 187-197.

Kim, H.-S., Kim, K.-S., Jung, S. S., Hwang, J. I., Choi, J.-S., & Sohn, I. (2015). Valorization of electric arc furnace primary steelmaking slags for cement applications. Waste management, 41, 85-93. doi:https://doi.org/10.1016/j.wasman.2015.03.019

Lu, X., Dai, W., Liu, X., Cang, D., & Zhou, L. (2019). Effect of basicity on cementitious activity of modified electric arc furnace steel slag. Metallurgical Research & Technology, 116(2), 217.

Mahoutian, M., Shao, Y., Mucci, A., & Fournier, B. (2015). Carbonation and hydration behavior of EAF and BOF steel slag binders. Materials and structures, 48(9), 3075-3085. doi:10.1617/s11527-014-0380-x

Mo, L., Zhang, F., Deng, M., Jin, F., Al-Tabbaa, A., & Wang, A. (2017). Accelerated carbonation and performance of concrete made with steel slag as binding materials and aggregates. Cement and Concrete Composites, 83, 138-145. doi:https://doi.org/10.1016/j.cemconcomp.2017.07.018

Motz, H., & Geiseler, J. (2001). Products of steel slags an opportunity to save natural resources. Waste management, 21(3), 285-293. doi:https://doi.org/10.1016/S0956-053X(00)00102-1

Muhmood, L., Vitta, S., & Venkateswaran, D. (2009). Cementitious and pozzolanic behavior of electric arc furnace steel slags. Cement and Concrete Research, 39(2), 102-109. doi:https://doi.org/10.1016/j.cemconres.2008.11.002

Ghadimi, M. j., and Naghipour, A. (2023). Investigating the Physical and Chemical Effects of Adding Electric Arc Furnace Slag in Different Percentages to Portland Cement. doi:http://dx.doi.org/10.2139/ssrn.4560899

Ouattara, D., Belem, T., Mbonimpa, M., & Yahia, A. (2018). Effect of superplasticizers on the consistency and unconfined compressive strength of cemented paste backfills. Construction and Building Materials, 181, 59-72.

Ouffa, N., Benzaazoua, M., Belem, T., Trauchessec, R., and Lecomte, A. (2023). An alternative to NaOH in the alkali-activation of ground granulated blast furnace slag in the formulation of cemented paste backfills. Paper presented at the Paste 2023: 25th International Conference on Paste, Thickened and Filtered Tailings, Banff. https://papers.acg.uwa.edu.au/p/2355_08_Belem/

Ouffa, N., Trauchessec, R., Benzaazoua, M., Lecomte, A., and Belem, T. (2022). A methodological approach applied to elaborate alkali-activated binders for mine paste backfills. Cement and Concrete Composites, 127, 104381. doi:https://doi.org/10.1016/j.cemconcomp.2021.104381

Roslan, N. H., Ismail, M., Abdul-Majid, Z., Ghoreishiamiri, S., and Muhammad, B. (2016). Performance of steel slag and steel sludge in concrete. Construction and Building Materials, 104, 16-24. doi:https://doi.org/10.1016/j.conbuildmat.2015.12.008

Roslan, N. H., Ismail, M., Khalid, N. H. A., and Muhammad, B. (2020). Properties of concrete containing electric arc furnace steel slag and steel sludge. Journal of Building Engineering, 28, 101060. doi:https://doi.org/10.1016/j.jobe.2019.101060

Sahi, A. (2016). Validation expérimentale d'un modèle de sélection optimale des liants dans la fabrication des remblais miniers cimentés. Mémoire de Maîtrise, Génie minéral, École Polytechnique de Montréal-UQAT, 196 p.

Scrivener, K., Martirena, F., Bishnoi, S., and Maity, S. (2018). Calcined clay limestone cements (LC3). Cement and Concrete Research, 114, 49-56.

Shi, C. (2005). Steel Slag — Its Production, Processing, Characteristics, and Cementitious Properties. Cheminform, 36. doi:10.1002/chin.200522249

Sun, X., Liu, J., Zhao, Y., Zhao, J., Li, Z., Sun, Y., Qiu, J., Zheng, P. (2022). Mechanical activation of steel slag to prepare supplementary cementitious materials: A comparative research based on the particle size

distribution, hydration, toxicity assessment and carbon dioxide emission. Journal of Building Engineering, 60, 105200. doi:https://doi.org/10.1016/j.jobe.2022.105200

Tariq, A., & Yanful, E. K. (2013). A review of binders used in cemented paste tailings for underground and surface disposal practices. Journal of environmental management, 131, 138-149.

Teo, P. T., Zakaria, S. K., Salleh, S. Z., Taib, M. A. A., Mohd Sharif, N., Abu Seman, A., Mohamed, J. J., Yusoff, M., Yusoff, A. H., Mohamad, M., Masri, M. N., and.Mamat, S. (2020). Assessment of Electric Arc Furnace (EAF) Steel Slag Waste's Recycling Options into Value Added Green Products: A Review. Metals, 10(10), 1347. Retrieved from https://www.mdpi.com/2075-4701/10/10/1347

Thomas, C., Rosales, J., Polanco, J. A., and Agrela, F. (2019). 7 - Steel slags. In J. de Brito and F. Agrela (Eds.), New Trends in Eco-efficient and Recycled Concrete (pp. 169-190): Woodhead Publishing.

Tossavainen, M., Engstrom, F., Yang, Q., Menad, N., Lidstrom Larsson, M., & Bjorkman, B. (2007). Characteristics of steel slag under different cooling conditions. Waste management, 27(10), 1335-1344. doi:https://doi.org/10.1016/j.wasman.2006.08.002

Yildirim, I. Z., and Prezzi, M. (2011). Chemical, mineralogical, and morphological properties of steel slag. Advances in Civil Engineering, 2011.

Yilmaz, E., Belem, T., Benzaazoua, M., and Bussière, B. (2010). Assessment of the modified CUAPS apparatus to estimate in situ properties of cemented paste backfill. Geotechnical Testing Journal, 33(5), 351-362.

Yilmaz, E., Belem, T., Bussière, B., and Benzaazoua, M. (2011). Relationships between microstructural properties and compressive strength of consolidated and unconsolidated cemented paste backfills. Cement and Concrete Composites, 33(6), 702-715.